Available online at www.sciencedirect.com
ScienceDirect
Mechanics of Materials 40 (2008) 206–219
MECHANICS OF MATERIALS
www.elsevier.com/locate/mechmat

Effects of mechanical properties and surface friction on elasto-plastic sliding contact

S.C. Bellemare [a,b], M. Dao [a], S. Suresh [a,*]

[a] *Department of Materials Science and Engineering, Massachusetts Institute of Technology, 77 Massachusetts Avenue, Cambridge, MA 02139, USA*
[b] *Simpson, Gumpertz & Heger, 41 Seyon Street, Suite 1-500, Waltham, MA 02453, USA*

Received 25 April 2007; received in revised form 31 July 2007

Abstract

Indentation hardness has been used extensively for material characterization and many recent computational studies have established quantitative relationships between elasto-plastic mechanical properties and the response in instrumented indentation. In contrast, very few studies have systematically quantified the effect of the plastic deformation characteristics on the frictional sliding response of metals and alloys. Building upon dimensional analysis and finite element computations, a parametric study was carried out to extend our previous work to different contact friction conditions. For a wide range of elasto-plastic and contact friction parameters, we established closed form universal functions, for various contact conditions, that relate elasto-plastic properties (Young's modulus, yield strength, and power law hardening exponent) to steady state frictional sliding response (scratch hardness, pile-up height and overall sliding frictional coefficient). Distribution of the plastic strain beneath the indenter was studied to rationalize the deformation modes versus elasto-plastic properties and pile-up. In parallel, experiments were conducted for the effect of plastic flow characteristics on the frictional sliding (or scratch) response under different surface friction conditions. Pure copper and a brass alloy were heat-treated to vary yield strength and strain hardening exponent and the contact friction coefficient was varied by applying a liquid lubricant on the surface. Frictional sliding experiments were conducted using a nanoindentation testing system, where grain size and alloy composition were found to influence the response. Although variations in the frictional sliding response versus yield strength, strain hardening and friction were invariably coupled, the combined computational and experimental approach enabled us to isolate the relative contributions of each parameter. The results clearly demonstrated that an increase in the strain hardening exponent can significantly decrease the pile-up height, with known and further potential implications for the evaluation of tribological damage.

Keywords: Frictional sliding; Scratch test; Elasto-plastic properties; Contact mechanics; Friction

1. Introduction

Material hardness is a mechanical property referring to the normal contact force that a material can support per projected unit area of contact. Indenta-

* Corresponding author. Tel.: +1 617 253 3320.
E-mail address: ssuresh@mit.edu (S. Suresh).

0167-6636/$ - see front matter © 2007 Elsevier Ltd. All rights reserved.
doi:10.1016/j.mechmat.2007.07.006

tion hardness tests have been used extensively for material characterization and also as a basis for predicting the tribological response (Hutchings, 1992; Fischer-Cripps, 2000; Gouldstone et al., 2007). Indentation tests were traditionally based on an estimate of the residual area of contact or the remnant penetration depth, but developments and commercialization of depth-sensing instrumented indentation systems have enabled continuous measurement of the force and displacement during loading and unloading. Following these advances, many studies have examined the contact mechanics of instrumented indentation. Dimensional analysis and finite element methods (FEM) were employed to quantify relationships between the measured force–displacement (P–h) response and elasto-plastic properties (Dao et al., 2001; Mata et al., 2002; Matsuda, 2002; Tunvisut et al., 2002; Bucaille et al., 2003; Chollacoop et al., 2003; Cao and Lu, 2004; Cheng and Cheng, 2004; Oliver and Pharr, 2004; Ogasawara et al., 2005; Wang et al., 2005). Other studies also investigated experimentally the indentation response of various materials using instrumented systems (Schwaiger et al., 2003; VanLandingham, 2003; Schuh and Nieh, 2004).

As compared to normal indentation, few studies have systematically investigated the mechanics for frictional sliding (Bucaille et al., 2001; Bucaille and Felder, 2002; Subhash and Zhang, 2002; Youn and Kang, 2004; Fang et al., 2005). In the steady state regime of frictional sliding, the normal force is maintained constant and the tangential displacement induces material flow and the formation of ridges or pile-ups on each side of the scratch scar. Under appropriate contact conditions, our related earlier computational study predicted a strong connection between the frictional sliding response and material elasto-plastic properties (Bellemare et al., 2007). In fact, the effects of initial yield strength and plastic strain hardening exponent were quantified and isolated for their contribution to scratch hardness and pile-up height. This quantitative approach to study frictional sliding was proposed as an experimental tool for material characterization, but also as a simple predictor for the tribological response of materials. Recently, a similar set of studies were carried out to determine and compare the hardness and friction response for a range of strain hardening characteristics (Wredenberg and Larsson, 2007). Their results showed a representative plastic strain of 35% for an indenter apex angle of 68° (Wredenberg and Larsson, 2007), versus 33.6% for an apex angle of 70.3° in our earlier study (Bellemare et al., 2007). Although these values are similar, our previous work indicated that the representative plastic strain is considerably smaller for high strain hardening materials. Several other previous experimental studies have used frictional sliding experiments (Zhang et al., 1994, 1995; Liang et al., 1995; Deuis et al., 1996; Wilson et al., 2000; Bolduc et al., 2003), but the underlying interpretation provided only partial information about the relative contributions to the overall frictional sliding response in terms of the material and contact parameters.

Contact friction significantly influences the sliding contact response. For a sliding contact where significant plastic deformation develops underneath the indented surface, we envision two components to the total or overall friction coefficient, which is defined as ratio of tangential force over normal force. The first component is from the local interaction between the indenter and material surfaces in normal contact, i.e. surface friction. This surface friction can be accounted for using Amontons's law with an appropriate friction coefficient and it can be directly affected by lubrication. The second component to the overall friction is from the work for plastically deforming the surface and it should be influenced by the contact geometry and elasto-plastic properties, although a recent study suggested independence on properties for relatively soft materials (Wredenberg and Larsson, 2007).

For normal indentation, FEM computations suggested a significant influence of the friction coefficient on the pile-up behavior (Mesarovic and Fleck, 1999; Carlsson et al., 2000; Mata and Alcala, 2004). Experimentally, lubricants decrease the indentation hardness (Atkinson and Shi, 1989; Shi and Atkinson, 1990) and increase the hardness in frictional sliding (Brookes and Green, 1979; Brookes, 1981). From the viewpoint of the contact geometry evolution, the frictional force pushes the material downward during normal indentation while it pushes the material upward and to the front and side in frictional sliding. This fundamental difference explains the reverse effect of friction in frictional sliding versus normal indentation, but a more detailed analysis is needed for a quantitative prediction of the effect of friction in sliding contact.

In the present study, we used dimensional analysis and large scale finite element computations, to extend our previous theoretical framework (Bellemare et al., 2007) to include the influence of various

contact friction conditions. We established a set of closed form universal functions to relate elasto-plastic properties, i.e. Young's modulus, yield strength and power law hardening exponent, to steady state frictional sliding response, i.e. scratch hardness, pile-up height and overall sliding frictional coefficient, with respect to various contact friction conditions. In parallel, we conducted a comprehensive set of sliding contact experiments on a model material system to investigate the effect of plastic flow characteristics and surface friction parameters on the frictional sliding response, or scratch response. The results are compared with predictions from our theoretical/computational results. Based on a comparison of experiments with computational results, the effect of plastic strain hardening on the deformation field is also discussed.

2. Experimental and computational methods

2.1. Material system

Copper was selected as a model material system because large variations in the strain hardening exponent can be introduced by controlling the grain size and composition. Commercially pure copper (99.9%) and a single phase copper–30 wt% zinc alloy were obtained from Noranda Inc. (Pointe-Claire, Canada) in the form of cold worked sheets that were 0.6 mm thick. Standard dog-bone specimens were machined out of the sheets. After machining, the specimens were divided into three groups that were then heat-treated for recrystallization at temperatures of 450, 600 or 700 °C for 3 h. The microstructure of each alloy was then characterized in detail, including a quantification of the average grain size $\bar{d}$ as listed in Table 1. With pure Cu and the brass alloy, a total of six material conditions were investigated. In the absence of other significant changes to the microstructure, the conditions with the different heat-treatments provided the opportunity to study the specific effect of the grain size on the frictional sliding response.

Table 1
Material conditions tested with average grain size, initial yield strength and strain hardening exponent based on tensile test results

Material	T (°C)	$\bar{d}$ (μm)	σ_y (MPa)	n
Cu	450	20 ± 8	145	0.13
Cu	600	150 ± 30	44	0.27
Cu	700	380 ± 50	28	0.29
Cu–Zn	450	27 ± 6	45	0.35
Cu–Zn	600	76 ± 10	15.5	0.41
Cu–Zn	700	180 ± 20	7	0.45

Tensile tests were carried out on all materials to quantify the plastic deformation response. Prior to testing, the specimens were marked with ink at specified interval distances to independently measure the plastic strain at maximum tensile strength. The stress–strain curves were corrected for machine/specimen compliance and consistency was obtained between the critical engineering strain, i.e. strain at tensile strength, and the permanent elongation of the specimens measured using the marking technique. True stress versus true strain power law hardening was used to fit the experimental data:

$$\sigma = \sigma_y \left(1 + \frac{E}{\sigma_y}\varepsilon_p\right)^n, \tag{1}$$

where ε_p is the equivalent plastic strain, σ_y is the initial yield strength, E is the Young's modulus of the material and n is the strain hardening exponent. The results from this fit are summarized in Table 1 and three example curves are shown in Fig. 1. In the fitting procedure, more weight was given to the later part of the experimental curve where the plastic strain is most significant.

2.2. The frictional sliding experiments

All specimens were mechanically polished to a surface roughness of less than ±5 nm and tested

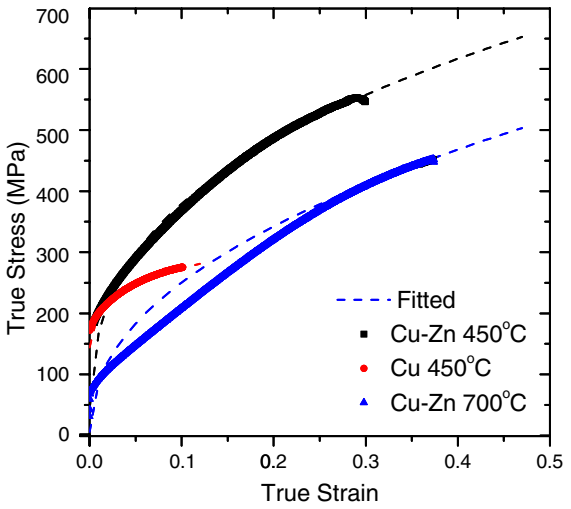

Fig. 1. True stress versus true strain curves for three different materials and the associated fitted function using power law strain hardening.

on a commercial nanoindentation test system (Nanotest™, Micro Materials Ltd., Wrexham, United Kingdom). The indenter was a conical diamond with an apex angle θ of 70.3° and a tip radius of 2 μm. For the conditions of penetration depth investigated, the size of the scratches was sufficiently large to consider the indenter as perfectly conical. The experiments were carried out under constant normal load, P, at a velocity of 10 μm/s and over a total distance of 1500 μm, which was sufficient to attain steady state conditions after approximately 300 μm and continue to generate a region of valid steady state profile. After the experiment, a series of at least 30 cross-sectional residual profiles were obtained over the steady state regime by using a Tencor P10 profilometer (KLA-Tencor, San Jose, California). The profilometer was equipped with a conical diamond probe which had an apex angle of 45° and a tip radius of 2 μm. The steady state regime was also observed with a Leo VP438 scanning electron microscope (Leo Electron Microscopy Inc., Thornwood, New York).

Schematic drawings of frictional sliding are shown in Fig. 2, where the frictional sliding process, a cross-sectional view of symmetry plane during the steady state stage, and a cross-sectional view of the residual scratch profile are presented. Graphical representations for the pile-up height h_p, the residual penetration depth h_r and the contact radius a_r are defined. The contact radius a_r can be used directly to calculate the overall resistance to penetration using the traditional definition of hardness (Tabor, 1951; Johnson, 1985; Williams, 1996; Fischer-Cripps, 2000; Gouldstone et al., 2007)

$$H_S = \frac{2P}{\pi a_r^2}, \tag{2}$$

where P is the applied normal load. Assuming the absence of significant size effects, the main advantage of the conical geometry is the size-independence due to self similarity. With this assumption, the simple ratio of h_p/h_r provides an indication on the tendency of the material to form a pile-up.

After hardness and pile-up profiles, friction is the third important parameter to the frictional sliding response. Because friction occurs at two different levels, we will separate the overall friction coefficient as

$$\mu_{tot} = \frac{F_t}{P} = \mu_a + \mu_w, \tag{3}$$

where F_t is the total tangential force, μ_a is the coefficient of friction for the normal contact and μ_w is the friction contribution besides μ_a. The parameter μ_a is governed by Amontons's law of friction which specifies the ratio between the normal pressure and the local tangential traction. The value of μ_a will be varied experimentally using an isostearic acid (Century 1105, Arizona Chemical, Jacksonville, Florida) as a liquid lubricant. The lubricant had a

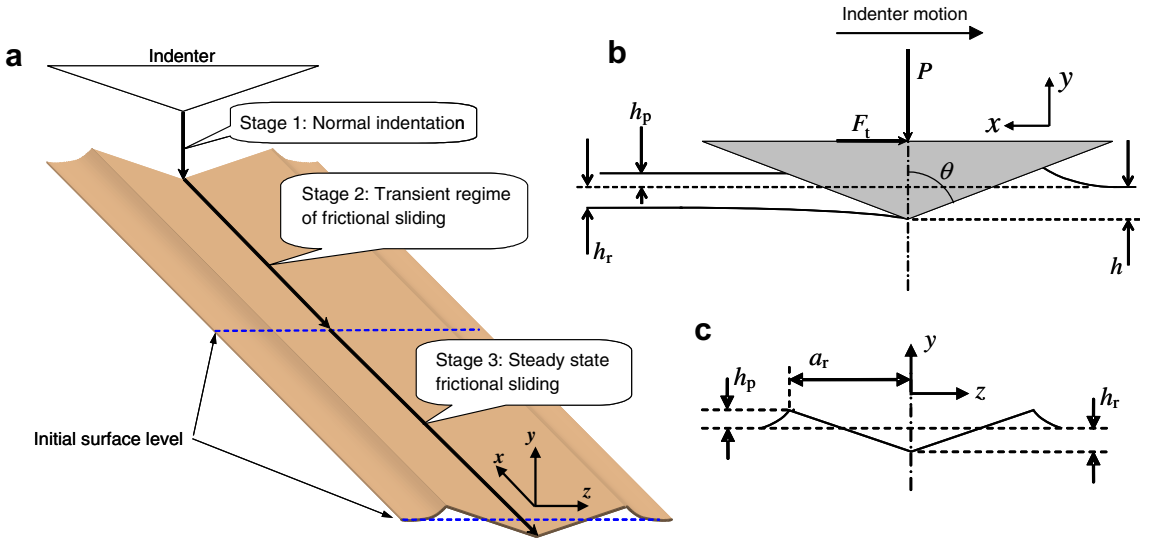

Fig. 2. (a) A schematic drawing of the frictional sliding process, (b) a cross-sectional of the symmetry plane in the steady state regime and (c) a cross-sectional view of the residual scratch profile. All solid lines represent the top free surface of the material being plastically deformed.

viscosity of 70 cps at 25 °C and it contained mainly C_{18} branched chains (59%) and C_{18} cyclic chains (11%).

2.3. Dimensional analysis and computational model setup

For steady state frictional sliding of elasto-plastic materials, the contact conditions can now be analyzed and predicted in detail. To simplify the elastic contributions from the material and the indenter, we used the reduced modulus (Johnson, 1985)

$$E^* = \left[\frac{(1-\nu^2)}{E} + \frac{(1-\nu_i^2)}{E_i}\right]^{-1}, \tag{4}$$

where E_i and ν_i are the Young's modulus and Poisson's ratio of the indenter, respectively. For the diamond indenter used in the experiments, $E_i = 1100$ GPa and $\nu_i = 0.07$ are given (MatWeb:www.matweb.com, 2006). The elastic constants specified for polycrystalline Cu were taken to be: $E = 110$ GPa and $\nu = 0.35$ (MatWeb:www.matweb.com, 2006). These properties were assumed to be isotropic for the conditions tested.

For a fixed cone apex angle of $\theta = 70.3°$ and a fixed friction coefficient of $\mu_a = 0.15$, three new dimensionless functions have been defined using dimensional analysis and evaluated numerically through a comprehensive parametric study (Bellemare et al., 2007). Under the assumptions for fixed θ and μ_a, these functions predict the frictional sliding response based on elasto-plastic properties and the following closed-form functions:

$$\Pi_\alpha\left(n, \frac{\sigma_y}{E^*}\right) = \left(\frac{H_S}{\sigma_y}\right) = \alpha 1(n) \Big/ \left(\frac{\sigma_y}{E^*}\right)^{\alpha 2(n)}, \tag{5}$$

$$\Pi_\beta\left(n, \frac{\sigma_y}{E^*}\right) = \frac{h_p}{h_r} = \Pi_{\beta,RP}(n) \Big/ \left[1 + \left(\frac{\sigma_y}{X_\beta(n)E^*}\right)^{p_\beta(n)}\right] \quad \text{and} \tag{6}$$

$$\Pi_\gamma\left(n, \frac{\sigma_y}{E^*}\right) = \left(\frac{F_t}{P}\right) = \mu_{tot} = \Pi_{\gamma,RP} \Big/ \left[1 + \left(\frac{\sigma_y}{X_\gamma(n)E^*}\right)^{p_\gamma(n)}\right], \tag{7}$$

where the subscript 'RP' indicate the value of the function at the limit of rigid-plastic properties, the variable F_t is for the overall lateral force and the variable μ_{tot} is for the overall friction coefficient. Simple numerical expressions were provided (Bellemare et al., 2007) for the other numerical terms for the sub-functions of $n(\alpha 1(n), \alpha 2(n), \Pi_{\beta,RP}(n), X_\beta(n), p_\beta(n), X_\gamma(n)$ and $p_\gamma(n))$ and the constant $\Pi_{\gamma,RP}$. All functions are smooth and with a monotonic variation, except $X_\beta(n)$ which has a minimum at $n = 0.4$. With these functions and their underlining assumptions, one can specify the elasto-plastic properties of a material and predict the frictional sliding response in terms of normalized scratch hardness $H_s/\sigma_y(\Pi_\alpha)$, ratio of pile-up height (Π_β) and overall friction coefficient $\mu_{tot}(\Pi_\gamma)$.

In their most general form, these dimensionless functions are expressed as:

$$\Pi_\alpha = f\left(n, \frac{\sigma_y}{E^*}, \mu_a, \theta\right), \tag{8}$$

$$\Pi_\beta = f\left(n, \frac{\sigma_y}{E^*}, \mu_a, \theta\right), \quad \text{and} \tag{9}$$

$$\Pi_\gamma = f\left(n, \frac{\sigma_y}{E^*}, \mu_a, \theta\right). \tag{10}$$

For the current study, we specifically investigate the effect of the friction coefficient μ_a, which will add a dimension to the dimensionless functions Π_α, Π_β and Π_γ presented in Eqs. (5)–(7). On the other hand, the parameter θ remains fixed at 70.3° in this study. Full three-dimensional models were used because the stress and strain fields generated by frictional sliding cannot be approximated using two-dimensional or axisymmetric FEM. The complete mesh domain contained 170,000 reduced integration 8-noded elements. The finite element computations were performed using the general purpose FEM software package ABAQUS (Simulia, Providence, Rhode Island, USA). The solution method was explicit and based on Eulerian boundaries where the mesh remains stationary. Additional details on the meshing procedure and model validation can be found elsewhere (Bellemare et al., 2007). The approach was well tested for mesh refinement and convergence, and for the independence of the solution method adapted.

Finite element solutions were obtained for fixed values of the friction coefficient $\mu_a = 0$, 0.08, 0.2 or 0.3. For the materials with a plastic strain hardening exponent $n \leqslant 0.2$, μ_a was limited to a maximum value of 0.2 (for $n < 0.35$) or 0.3 (for $n > 0.35$) because higher μ_a could generate physical and numerical instability due to excessive pile-up. In the complete parametric study a minimum of 6 cases of σ_y/E^* were explored for any combination of n and μ_a covered, adding a total of 90 cases to the previous study (Bellemare et al., 2007) that focused on $\mu_a = 0.15$. The same procedure as in the previous

study was used to extract h_p, h_r and a_r from the nodal position of the residual profile. The FEM results from both studies were all incorporated into the new dimensionless functions so as to develop a comprehensive understanding of the effects of E^*, σ_y, n and μ_a on frictional sliding.

3. Results and discussion

3.1. Quantitative descriptions of contact sliding with friction

Extending our previous study (Bellemare et al., 2007), we now consider the effect of varying friction coefficient μ_a on the sliding contact response. Computationally, three parameters can be varied independently: the friction coefficient μ_a, the normalized initial yield strength σ_y/E^*, and the strain hardening exponent n. We quantified the effect of each of these parameters within the framework of the general dimensionless functions Π_α, Π_β and Π_γ (Eqs. (8)–(10)). Although we could have used new functions to represent the new data, we found that the general dependency on n and σ_y/E^* was very similar to that in our earlier analysis (Eqs. (4)–(7)). Therefore, the influence of the friction coefficient was incorporated by adding penalty terms in the former equations (Bellemare et al., 2007). The new sub-functions and their coefficients were determined by minimization of the residuals. These universal dimensionless functions represent fits to the FEM results, and the constructed fitting functions will be compared with and verified against experimental measurements for a range of cases in Section 3.2.

For the normalized scratch hardness H_S/σ_y, the best fit was obtained by using the function

$$\Pi_\alpha = \left(\frac{H_S}{\sigma_y}\right) = [\alpha 1(n) + n\Gamma_{\alpha 1}(\mu_a)]\left(\frac{\sigma_y}{E^*}\right)^{[\alpha 2(n)+\Gamma_{\alpha 2}(\mu_a)]} \quad (11)$$

with

$$\Gamma_{\alpha 1}(\mu_a) = 0.12 - 0.64/[1 + e^{30(\mu_a - 0.1)}],$$
$$\Gamma_{\alpha 2}(\mu_a) = 0.006 - 0.0278/[1 + e^{25(\mu_a - 0.1)}]$$

and the sub-functions ($\alpha 1(n)$ and $\alpha 2(n)$) as evaluated previously (Bellemare et al., 2007). For hardness, the contribution from the friction coefficient μ_a is included with the terms that previously depended only on the strain hardening exponent n. The sub-functions $\Gamma_{\alpha 1}$ and $\Gamma_{\alpha 2}$ are exponential growth functions and their values vary monotonically with μ_a. They were selected to minimize the error when fitting all the data throughout the range of numerically simulated material properties.

Fig. 3 presents the function Π_α and the associated FEM data points on log–log plots of the normalized hardness H_S/σ_y versus the normalized yield strength σ_y/E^*. The data for the five different values of the strain hardening exponent n are well separated. For each value of n the effect of the surface friction coefficient μ_a is more limited, but the following trends are seen:

- For $n \cong 0.35$, the effect of friction is negligible;
- For $n > 0.35$, the hardness increases with increasing friction coefficient μ_a;
- For $n < 0.35$, the hardness decreases with increasing friction coefficient μ_a.

For $n < 0.35$, the decrease in hardness could be due to an increase in the amount of material being pushed to the side of indenter, increasing the area of contact through a higher pile-up. Although the changes appear limited on this log–log plot, the effect on hardness can reach 5–15% depending on the conditions.

The second function studied is Π_β for the normalized pile-up height h_p/h_r. The behavior of this function should be asymptotic on both sides with little influence of yield strength for rigid-plastic materials and with a residual height of zero in the

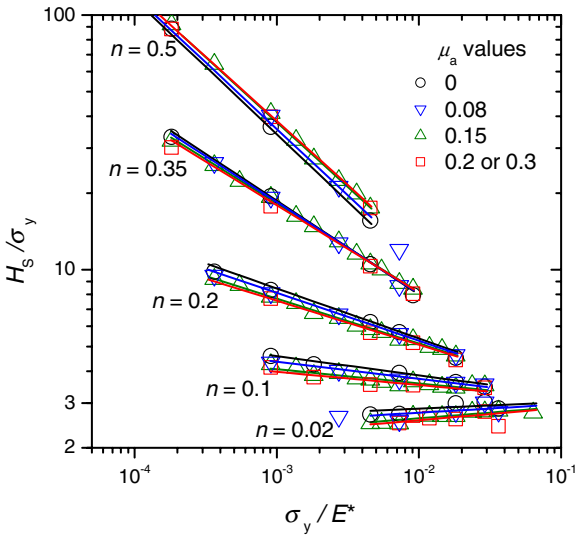

Fig. 3. Effect of the friction coefficient μ_a on the normalized hardness versus normalized yield strength relationship.

elastic limit. The logistic function selected in previous study respects both of these limits and it allows for a simple expression of the pile-up height:

$$\Pi_\beta = \frac{h_p}{h_r} = \Pi_{\beta,RP}(n)\Gamma_{\beta,RP}(\mu_a) \Bigg/ \left[1 + \left(\frac{\sigma_y}{X_\beta(n)\Gamma_{X\beta}(\mu_a)E^*}\right)^{p_\beta(n)}\right] \tag{12}$$

with

$$\Gamma_{\beta,RP}(\mu_a) = 0.909 + 0.627\mu_a,$$
$$\Gamma_{X\beta}(\mu_a) = 0.651 + 1.21\mu_a + 7.61\mu_a^2,$$

and the sub-functions of n ($\Pi_{\beta,RP}(n)$, X_β (n) and $p_\beta(n)$) as evaluated previously (Bellemare et al., 2007). Fig. 4 presents the function Π_β evaluated at the different values of n and μ_a for which we have FEM results. The sets of curves for the specified values of n illustrate in more detail the combined influence of n and σ_y/E^* on h_p/h_r. Within each set of these curves, the normalized pile-up height h_p/h_r always increases when the friction coefficient μ_a increases. This increase in height can be associated with an increase in the interaction forces that push the material to the front and sides of the indenter.

The absolute value of the offset in h_p/h_r caused by variations in μ_a is significant for the strain hardening exponent range: $0.02 \leqslant n \leqslant 0.35$. For the largest value of $n = 0.5$, where the transition between pile-up and sink-in is approached, the effect of friction is limited. The sink-in phenomenon is a different behavior than the pile-up behavior reported in this paper because the motion of the plastically deforming material is all downward ahead of the tip. This sink-in was observed during simulation for $n = 0.5$ and $\sigma_y/E^* > 0.005$, but the results are not presented here. With sink-in, there is no real pile-up and it is difficult to ascertain the area of contact from the residual profile. Including sink-in behavior in the equations would require a more detailed analysis. At the same time, it would probably find limited practical applications because very few hardened ductile materials have properties beyond the range covered in this study.

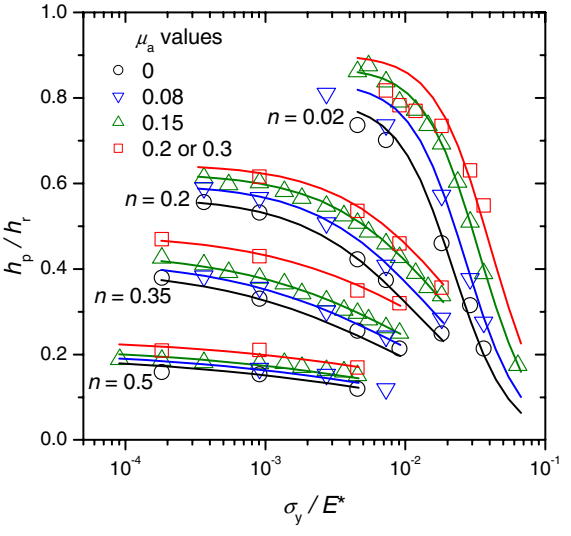

Fig. 4. Effect of the frictional coefficient μ_a on the normalized pile-up height versus normalized yield strength relationship.

To illustrate the effect of the strain hardening exponent on the pile-up, a semi-quantitative description was developed for the evolution of the deformation zone with plastic properties. Data for the equivalent plastic strain were extracted from the elements located in the unloaded region and at a distance $a_r/2$ from the symmetry plane and they are reported in Fig. 5 as a function of the distance beneath the scratch surface. Fig. 5a presents a series of equivalent plastic strain contour plots for a relatively soft material where $\sigma_y/E^* = 0.001$. As the strain hardening exponent decreases, the equivalent plastic strain near the surface increases significantly. For the strain distribution beneath the surface, the plastic strain deceases less rapidly for the materials with a higher hardening exponent. The plastic strain is more distributed with increasing n, which is consistent with the decrease in the pile-up height as the flow of material extends further beneath material/indenter interface.

The initial yield strength also influences the plastic strain distribution. Fig. 5b presents a similar series of results for a harder material where $\sigma_y/E^* = 0.01$. Although the general shape of these curves remains the same as those for the softer material, there is a general and significant decrease in the magnitude of the plastic strain. When used together, Fig. 5a and b provide a description of the evolution of equivalent plastic strain for different strain hardening exponent and initial yield strength values. The hardening exponent significantly affects the distribution, while the initial yield strength clearly influences the average magnitude of the equivalent plastic strain.

The third and last universal function Π_γ is for the overall friction coefficient μ_{tot} or the ratio of the lateral force of interaction F_t over the normal force P between the indenter and the surface. The effect of friction was incorporated to yield

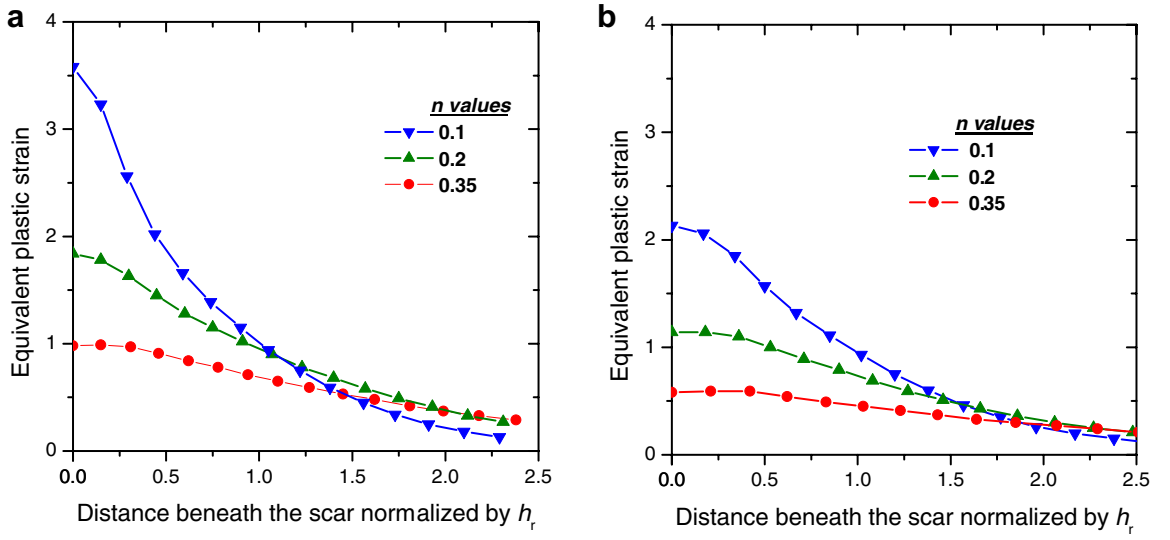

Fig. 5. Magnitude of the equivalent plastic strain beneath the indenter for (a) $\sigma_y/E^* = 0.001$ and (b) $\sigma_y/E^* = 0.01$.

$$\Pi_\gamma = \left(\frac{F_t}{P}\right) = \mu_{tot} = \mu_a + \mu_w = \mu_a + (\Pi_{\gamma,RP}\Gamma_{\gamma,RP}(\mu_a) - \mu_a) \Bigg/ \left[1 + \left(\frac{\sigma_y}{X_\gamma(n)\Gamma_{X\gamma}(\mu_a)E^*}\right)^{p_\gamma(n)}\right] \quad (13)$$

with

$$\Gamma_{\gamma,RP}(\mu_a) = 0.586 + 2.6\mu_a + 0.877\mu_a^2,$$
$$\Gamma_{X\gamma}(\mu_a) = 0.8 + 1.33\mu_a + 0.235\mu_a^2$$

and the sub-functions of n ($\Pi_{\gamma,RP}$, $X_\gamma(n)$ and $p_\gamma(n)$) as evaluated previously (Bellemare et al., 2007). Without losing generality, μ_{tot} is defined to be the sum of two contributions from the quantities μ_a and μ_w (see Eq. (3)), where μ_w encompasses all contributions to the lateral force that cannot be accounted for by Amontons's law of friction with a coefficient μ_a evaluated from the nominally elastic contact between two bodies. Therefore, μ_w accounts for all increases in F_t that are required to deform the material plastically and to move it under and to the side of the indenter, leaving the path for the advancing indenter. Consequently, μ_w is the only term in the equation that depends on mechanical properties.

Fig. 6 graphically represents the function Π_γ where the sets of adjacent curves are now for a given value of the friction coefficient μ_a and the different series are for the five different values of μ_a. The curves were plotted using Eq. (9) while the FEM data points are also included to illustrate the fitting

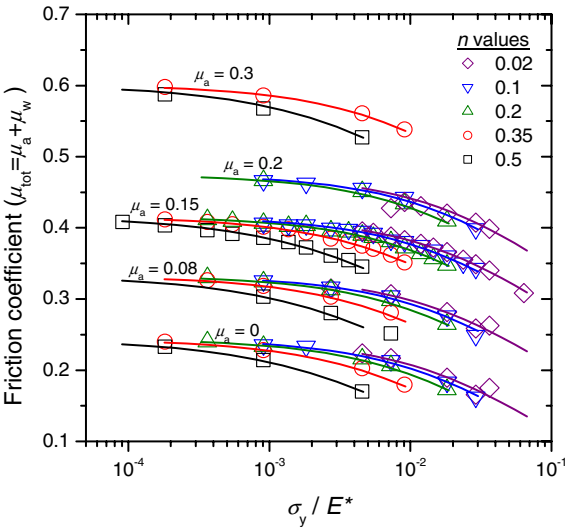

Fig. 6. Effect of the frictional coefficient μ_a on the overall friction coefficient versus normalized yield strength relationship.

accuracy. Although the effect of material properties on the geometrical friction coefficient is smaller than the pile-up height, the variations over the range studied are still significant. The large range of material parameters used in the current study is probably the origin for the discrepancy between the effect of friction that we found and other published results where the effect of material parameters on geometrical friction was found limited over a narrower range of elasto-plastic properties (Wredenberg and

Larsson, 2007). It is evident that, for a given set of elasto-plastic properties, the μ_w term consistently increases with μ_a. Another feature that persists for the different values of μ_a is that friction is independent of yield strength and strain hardening exponent at the limit of a rigid-plastic material.

3.2. Experimental results and correlations with computational results

An experimental study was undertaken to measure and control the friction coefficient. The value of μ_a was measured through a repeated frictional sliding test in which a spherical tip with a radius of 100 μm was used for repeatedly sliding over the same area 12 times. The normal load P was fixed at 1 N and the material was a high strength specimen of pure copper with an indentation hardness of 1.5 GPa. Under those conditions, the ratcheting or deepening of the impression progressively reduced and became negligible after approximately 8 passes. Fig. 7 shows the raw friction signal obtained during such an experiment. The friction coefficient is found to decrease from an initial value of approximately 0.22 for the first pass to a steady state value of approximately 0.14. This technique of measuring μ_a may result in a small overestimation with a potential for a limited amount of plasticity in steady state, but it offers a reasonable estimate of μ_a in an efficient manner.

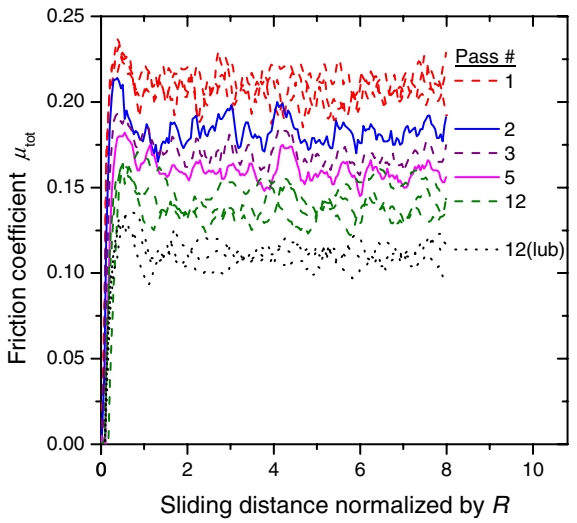

Fig. 7. Experimental determination of the friction coefficient μ_a. From top to bottom the curves represent the coefficient of friction μ_{tot} for an increasing number of passes over the same area until a steady state is reached. The dotted lime at the bottom is for the steady state with lubrication.

To vary experimentally μ_a, we used the isostearic acid as a liquid lubricant. The lubricant was added to the surface and the tip after carrying out the load and displacement calibrations. With the relatively small velocity of the tip, the conditions were boundary lubrication. To verify the influence on μ_a, the experiment with a spherical tip presented in Fig. 7 was followed by another experiment under the same conditions but with lubricant. For each pass, the friction coefficient was significantly lower with a lubricant and Fig. 7 presents the results for the steady state regime. The use of lubrication caused the steady state friction coefficient to decrease from 0.14 to 0.11. This 25% decrease could have several beneficial effects including a reduction in chip formation on hard materials with limited plastic strain hardening exponent. The variation also allows for a more comprehensive comparison between computational predictions and experimental results.

After measuring experimentally the surface friction coefficient, we performed frictional sliding experiments with the conical tip. The tests were on pure Cu and Cu–Zn, at a normal load $P = 2$ N, and for both the unlubricated and the lubricated cases. For each material condition, the experiment was repeated five times and profilometry was carried out on each profile. From these profiles, the scratch parameters were calculated and compared with predictions using the dimensionless functions, Eqs. (11)–(13). For each of the three parameters under the unlubricated condition, Table 2(panel a) indicates a maximum difference between the experiment and the predictions of at most 7%, 13% and 5% for the hardness, pile-up and friction, respectively. In addition, the differences between experiments and predictions indicate the absence of a definite trend, suggesting that the overall dependence of sliding behavior on elasto-plastic properties is correctly predicted over the range of properties studied. Similarly, Table 2(panel b) shows the maximum difference of 11% for lubricated case for hardness and pile-up ratio between experiments and predictions.

The effect of different friction coefficients on normalized pile-up height is summarized in Fig. 8. The materials shown in Fig. 8 are classified by their value of the strain hardening exponent n. The values of the pile-up height is consistently lower with a lubricant, but the effect of lubrication is found to progressively decrease with increasing n and

Table 2
Experimental results compared with the predictions made using the dimensionless functions: (a) unlubricated friction ($\mu_a = 0.14$) and (b) lubricated friction ($\mu_a = 0.11$)

Material (treatment T in °C)	Properties		H_S (GPa)			h_p/h_r			μ_{tot}		
(*a*)	σ_y (MPa)	n	Exp.	FEM	Δ (%)	Exp.	FEM	Δ (%)	Exp.	FEM	Δ (%)
Cu(450)	145	.13	0.66	0.71	−7	.7	0.69	3	.42	.406	3
Cu(600)	44	.27	0.62	0.66	−6	.57	0.52	13	.43	.409	5
Cu(700)	28	.29	0.60	0.55	−1	.51	0.50	5	.42	.410	2
Cu–Zn(450)	45	.35	1.13	1.16	−3	.44	0.40	12	.41	.407	1
Cu–Zn(600)	15.5	.41	0.95	0.90	5	.3	0.33	−8	.40	.410	−2
Cu–Zn(700)	7	.45	0.81	0.78	4	.28	0.28	1	.41	.411	0

Material (T in °C)	Properties		H_S (GPa)			h_p/h_r		
(*b*)	σ_y (MPa)	n	Exp.	FEM	Δ (%)	Exp.	FEM	Δ (%)
Cu (450)	145	.13	0.71	0.73	−2	0.63	0.68	−7
Cu (600)	44	.27	0.70	0.67	4	0.47	0.50	−7
Cu (700)	28	.29	0.62	0.56	11	0.45	0.49	−7
Cu–Zn (450)	45	.35	1.19	1.17	2	0.41	0.39	4
Cu–Zn (600)	15.5	.41	0.92	0.91	1	0.29	0.33	−11
Cu–Zn (700)	7	.45	0.78	0.78	0	0.28	0.28	1

The materials are listed in order of increasing n.

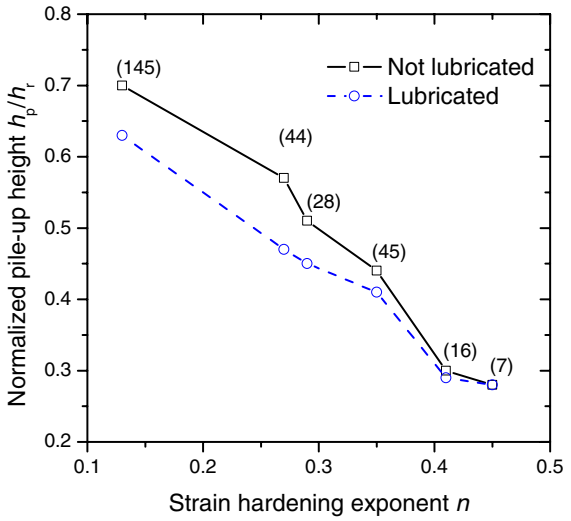

Fig. 8. Influence of lubrication on the experimentally measured values of the pile-up height. The numbers in parenthesis are the values of the initial yield strength in units of MPa for each case.

eventually vanish for $n = 0.5$. For the scratch hardness, the results presented in Table 2(panel b) are consistent with the predictions from the simulation for n below 0.35 where the hardness increased with decreasing μ_a. Above $n = 0.35$, a decrease in hardness was observed for all three Cu–Zn alloys to an extent slightly larger than that predicted computationally.

The overall coefficient of friction μ_{tot} can be measured readily using an instrumented nanoindenter wherein the frictional sliding experiment is performed. For all six ductile materials investigated, Table 2(panel a) shows a maximum difference of less than 7% in the value of μ_{tot}. A reasonable agreement was obtained between the experiments and the predictions. However, at least for the range of conditions studied, it would be difficult to use only the friction information to differentiate between the materials. A similar observation was also made from a previous study on nickel where the effect of grain-size refinement and large variations in yield strength did not significantly change the overall friction coefficient (Bellemare et al., 2007). Although the friction coefficient μ_{tot} can be readily monitored during an experiment, the two scratch parameters that are most sensitive to elasto-plastic properties are definitely the hardness and the normalized pile-up height. In other words, for the conditions explored in this work, relatively little variation in overall friction coefficient was found.

For illustration purposes, we now extract representative experimental pile-up profiles from the different conditions listed in Table 2 and discuss them with respect to the dimensionless functions. As listed in Table 2, with the same heat-treatment condition, the pile-up height is always lower in Cu–Zn than in pure Cu. From the dimensionless function in Eq. (12), a decrease in yield strength, as seen with Cu–Zn, is predicted to always increase the pile-up height. Therefore, any significant decrease

in pile-up height observed with Cu–Zn is necessarily due to the increase in the strain hardening exponent because the initial yield strength is lower for Cu–Zn and a lower yield strength would normally increase the pile-up. This experimental comparison suggests a dominant effect of the strain hardening exponent. It is also in agreement with Eq. (12) that predicts a limited sensitivity of pile-up height on the initial yield strength σ_y for the range of elasto-plastic properties covered in this study. Therefore, in the following discussion, we primarily focus on the variation of n to interpret the results from these experiments.

A strong correlation can be identified between the strain hardening exponent n and the normalized pile-up height. Fig. 9a presents five individual residual profiles for each of the two materials recrystallized at the lowest temperature of 450 °C, a condition for which n is 0.13 for pure Cu and 0.35 for Cu–Zn. On this figure, the direction of motion of the indenter is normal to the plane of the image. Although the profiles of the two materials are similar in general shape, the average value of h_p/h_r decreases from 0.70 to 0.44 as n increases from 0.13 to 0.35. Similarly, Fig. 9b presents profiles for recrystallization at the highest temperature where n is 0.29 for pure Cu and 0.45 for Cu–Zn. With the decrease in n between pure Cu and Cu–Zn, the average h_p/h_r decreases by nearly one half, from 0.51 to 0.28. With an experimental scatter in height of the order of ±0.05 and excellent reproducibility between the different scratches, the differences between pure Cu and Cu–Zn are significant and well beyond the level of fluctuations and consistent with the finite element predictions. For these two specific examples, the initial yield strength of the material was lower for the high hardening case, which would have increased the pile-up height based on Eq. (12). Therefore, the decrease in h_p/h_r can only be due to the increase in n. In fact, the decrease and variation between the conditions shown in Fig. 9 would have been even more significant without the difference in initial yield strength between the materials. Thus, the effects of n alone would be higher than the differences shown in Fig. 9.

Fig. 10 presents secondary electron images obtained in a scanning electron microscope (SEM). For each of the four material conditions, the images present the steady state regime and the final termination of the experiment for an indenter moving downward. In the steady state regime, the pile-up is more regular for the samples recrystallized

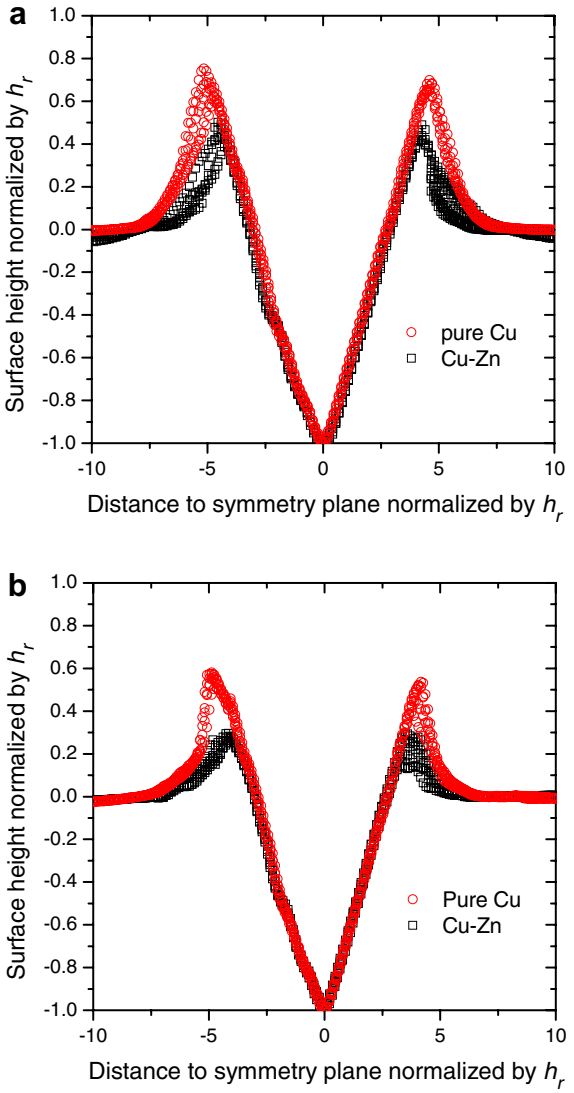

Fig. 9. Cross-section profiles for the experiments on the materials recrystallized at (a) the lowest temperature of 450 °C and (b) the highest temperature of 700 °C. There are five data sets for each of the two materials.

at 450 °C than for those recrystallized at 700 °C. At least in Cu–Zn, the preferential orientation of the deformation bands illustrates an effect of individual grains. For pure Cu recrystallized at 700 °C, there are also changes in the orientation of the bands on the free surface that are consistent with the intrinsic effect of grains. Since the grains are larger for the highest recrystallization temperature of 700 °C, the intrinsic effect of grains with different orientations could well explain the variability in scar width and surface features.

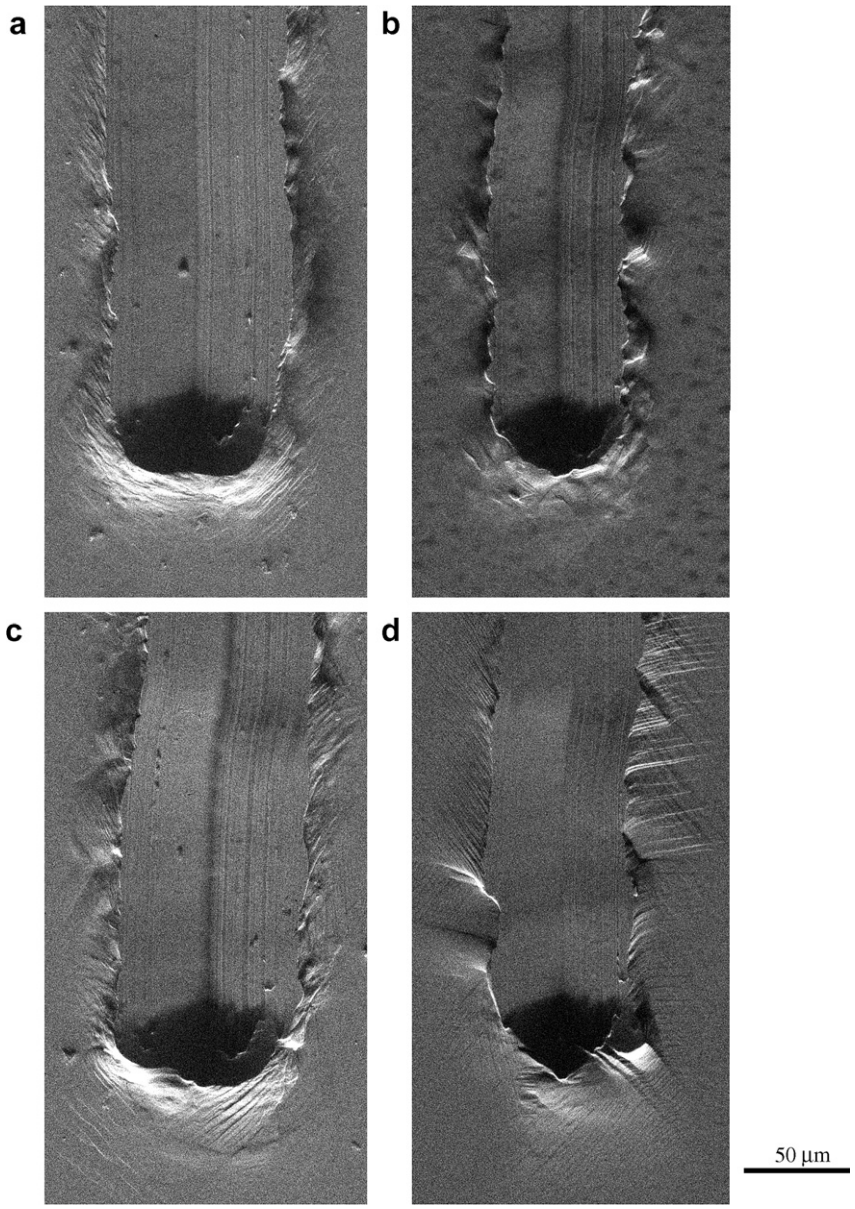

Fig. 10. Top surface image over the steady regime and the termination of a scratch for: (a) pure Cu recrystallized at 450 °C, (b) Cu–Zn also at 450 °C, (c) pure Cu at 700 °C and (d) Cu–Zn also at 700 °C. The indenter was traveling from top to bottom.

Intrinsic effects from the microstructure caused local fluctuations in the scratch pattern, including scar width and pile-up height. However, it should be noted that the average values remained consistent with the FEM predictions which are based on a continuum formulation. Due to the lateral displacement, frictional sliding offers the advantage over normal indentation to probe a larger volume of material and can generate averaged values of elasto-plastic properties from a single experiment.

4. Conclusions

The frictional sliding contact of elasto-plastic materials was studied experimentally and computationally. The following conclusions can be drawn:

1. High plastic strain hardening significantly decreases the normalized pile-up height for the material left on each side of the scratch scar. A more refined grain microstructure reduces the

variability in the frictional sliding process, and it also decreases the normalized pile-up height.
2. High plastic strain hardening or yield strength decreases the magnitude of the equivalent plastic strain underneath the indenter. Strain hardening also distributes the strain to a greater distance beneath the surface of contact.
3. Dimensionless functions developed in our parallel study (Bellemare et al., 2007) on instrumented frictional sliding were modified to include the effect of the friction coefficient. For materials for which the strain hardening exponent is below 0.35, scratch hardness increases if friction decreases.
4. The most significant effect of friction is to increase the normalized pile-up height. The effect decreases for very large strain hardening exponents. No previous studies had reported the specific effect of friction on the frictional sliding response of a large variety of materials.
5. An isostearic acid used as a boundary lubricant can decrease by 25% the friction coefficient between the surface and the diamond tip. The experimental effect of lubrication on the hardness and pile-up was consistent with our finite element predictions.

The frictional sliding experiment can be well controlled and designed to consistently yield results in agreement with the computational predictions. It could become an alternative or a complement to a normal indentation test.

Acknowledgements

The authors would like to acknowledge the financial support of the Defense University Research Initiative on Nano Technology (DURINT) which is funded at MIT by ONR under grant N00014-01-1-0808, as well as a research grant provided by Schlumberger Limited. Post-Graduate Fellowship from the Natural Science and Engineering Research Council of Canada is also acknowledged. Finally, special thanks to Professor Ivan Dickson from Ecole Polytechnique de Montreal for coordinating the supply of the materials used for this study.

References

Atkinson, M., Shi, H., 1989. Friction effect in low load hardness testing of iron. Materials Science and Technology 5 (6), 613–614.

Bellemare, S., Dao, M., Suresh, S., 2007. The frictional sliding response of elasto-plastic materials in contact with a conical indenter. International Journal of Solids and Structures 44 (6), 1970–1989.

Bolduc, M., Terreault, B., Reguer, A., Shaffer, E., St-Jacques, R.G., 2003. Optimum tribological improvement of aluminum using oxygen plasma source ion implantation. Journal of Materials Research 18 (8), 1761–1764.

Brookes, C.A., 1981. Scratch and indentation hardness of crystals. Philosophical Magazine A 43 (3), 529–543.

Brookes, C.A., Green, P., 1979. Anisotropy in the scratch hardness of cubic crystals. Proceedings of the Royal Society of London Series A – Mathematical and Physical Sciences 368 (1732), 37–57.

Bucaille, J.L., Felder, E., 2002. Finite-element analysis of deformation during indentation and scratch tests on elastic-perfectly plastic materials. Philosophical Magazine A – Physics of Condensed Matter Structure Defects and Mechanical Properties 82 (10), 2003–2012.

Bucaille, J.L., Felder, E., Hochstetter, G., 2001. Mechanical analysis of the scratch test on elastic perfectly plastic materials with the three-dimensional finite element modeling. Wear 249 (5–6), 422–432.

Bucaille, J.L., Stauss, S., Felder, E., Michler, J., 2003. Determination of plastic properties of metals by instrumented indentation using different sharp indenters. Acta Materialia 51 (6), 1663–1678.

Cao, Y.P., Lu, J., 2004. Depth-sensing instrumented indentation with dual sharp indenters: stability analysis and corresponding regularization schemes. Acta Materialia 52 (5), 1143–1153.

Carlsson, S., Biwa, S., Larsson, P.-L., 2000. On frictional effects at inelastic contact between spherical bodies. International Journal of Mechanical Sciences 42 (1), 107–128.

Cheng, Y.T., Cheng, C.M., 2004. Scaling, dimensional analysis, and indentation measurements. Materials Science & Engineering R-Reports 44 (4–5), 91–149.

Chollacoop, N., Dao, M., Suresh, S., 2003. Depth-sensing instrumented indentation with dual sharp indenters. Acta Materialia 51 (13), 3713–3729.

Dao, M., Chollacoop, N., Van Vliet, K.J., Venkatesh, T.A., Suresh, S., 2001. Computational modeling of the forward and reverse problems in instrumented sharp indentation. Acta Materialia 49 (19), 3899–3918.

Deuis, R.L., Subramanian, C., Yellup, J.M., 1996. Abrasive wear of aluminium composites – a review. Wear 201 (1–2), 132–144.

Fang, L., Cen, Q., Sun, K., Liu, W., Zhang, X., Huang, Z., 2005. FEM computation of groove ridge and Monte Carlo simulation in two-body abrasive wear. Wear 258 (1–4 SPEC ISS), 265–274.

Fischer-Cripps, A.C., 2000. Introduction to Contact Mechanics. Springer-Verlag, New York.

Gouldstone, A., Chollacoop, N., Dao, M., Li, J., Minor, A.M., Shen, Y.-L., 2007. Indentation across size scales and disciplines: recent developments in experimentation and modeling. Acta Materialia 55 (12), 4015–4039.

Hutchings, I.M., 1992. Tribology: Friction and Wear of Engineering Materials. CRC Press, Kent.

Johnson, K.L., 1985. Contact Mechanics. Cambridge University Press, London.

Liang, Y.N., Ma, Z.Y., Li, S.Z., Li, S., Bi, J., 1995. Effect of particle size on wear behaviour of sic particulate-reinforced

aluminum alloy composites. Journal of Materials Science Letters 14 (2), 114–116.
Mata, M., Alcala, J., 2004. The role of friction on sharp indentation. Journal of the Mechanics and Physics of Solids 52 (1), 145–165.
Mata, M., Anglada, M., Alcala, J., 2002. A hardness equation for sharp indentation of elastic-power-law strain-hardening materials. Philosophical Magazine A: Physics of Condensed Matter, Structure, Defects and Mechanical Properties 82 (10 SPEC), 1831–1839.
Matsuda, K., 2002. Prediction of stress–strain curves of elastic–plastic materials based on the vickers indentation. Philosophical Magazine A: Physics of Condensed Matter, Structure, Defects and Mechanical Properties 82 (10 SPEC), 1941–1951.
MatWeb: www.matweb.com, 2006. Material Property Data. Automation Creations, Inc.
Mesarovic, S.D., Fleck, N.A., 1999. Spherical indentation of elastic–plastic solids. Proceedings of the Royal Society of London Series A – Mathematical Physical and Engineering Sciences 455 (1987), 2707–2728.
Ogasawara, N., Chiba, N., Chen, X., 2005. Representative strain of indentation analysis. Journal of Materials Research 20 (8), 2225–2234.
Oliver, W.C., Pharr, G.M., 2004. Measurement of hardness and elastic modulus by instrumented indentation: advances in understanding and refinements to methodology. Journal of Materials Research 19 (1), 3–20.
Schuh, C.A., Nieh, T.G., 2004. A survey of instrumented indentation studies on metallic glasses. Journal of Materials Research 19 (1), 46–57.
Schwaiger, R., Moser, B., Dao, M., Chollacoop, N., Suresh, S., 2003. Some critical experiments on the strain-rate sensitivity of nanocrystalline nickel. Acta Materialia 51 (17), 5159–5172.
Shi, H., Atkinson, M., 1990. A friction effect in low-load hardness testing of copper and aluminum. Journal of Materials Science 25 (4), 2111–2114.
Subhash, G., Zhang, W., 2002. Investigation of the overall friction coefficient in single-pass scratch test. Wear 252 (1–2), 123–134.
Tabor, D., 1951. The Hardness of Metals. Clarendon press, Oxford.
Tunvisut, K., Busso, E.P., O'Dowd, N.P., Brantner, H.P., 2002. Determination of the mechanical properties of metallic thin films and substrates from indentation tests. Philosophical Magazine A: Physics of Condensed Matter, Structure, Defects and Mechanical Properties 82 (10 SPEC), 2013–2029.
VanLandingham, M.R., 2003. Review of instrumented indentation. Journal of Research of the National Institute of Standards and Technology 108 (4), 249–265.
Wang, L., Ganor, M., Rokhlin, S.I., 2005. Inverse scaling functions in nanoindentation with sharp indenters: determination of material properties. Journal of Materials Research 20 (4), 987–1001.
Williams, J.A., 1996. Analytical models of scratch hardness. Tribology International 29 (8), 675–694.
Wilson, S., Hawthorne, H.M., Yang, Q., Troczynski, T., 2000. Sliding and abrasive wear of composite sol–gel alumina coated al alloys. Surface and Coatings Technology, 389–396.
Wredenberg, F., Larsson, P.-L., 2007. On the numerics and correlation of scratch testing. Journal of Mechanics of Materials and Structures 2 (3), 573–594.
Youn, S.W., Kang, C.G., 2004. A study of nanoscratch experiments of the silicon and borosilicate in air. Materials Science and Engineering A 384 (1–2), 275–283.
Zhang, Z., Zhang, L., Mai, Y.-W., 1994. Modelling friction and wear of scratching ceramic particle-reinforced metal composites. Wear 176 (2), 231–237.
Zhang, Z.F., Zhang, L.C., Mai, Y.-W., 1995. Particle effects on friction and wear of aluminium matrix composites. Journal of Materials Science 30 (23), 5999–6004.